Renewable Energy 146 (2020) 1659–1666

Contents lists available at ScienceDirect

Renewable Energy

journal homepage: www.elsevier.com/locate/renene

Enhancing the efficiency of mixed halide mesoporous perovskite solar cells by introducing amine modified graphene oxide buffer layer

Çiğdem Şahin [a], Halide Diker [b], Dimitra Sygkridou [c], Canan Varlikli [b, *], Elias Stathatos [c, **]

[a] Department of Chemistry, Art & Science Faculty, Pamukkale University, Denizli, Turkey
[b] Department of Photonics, Izmir Institute of Technology, 35430, Urla, Izmir, Turkey
[c] Nanotechnology and Advanced Materials Laboratory, Electrical and Computer Engineering Department, University of the Peloponnese, 26334, Patras, Greece

ARTICLE INFO

Article history:
Received 29 October 2018
Received in revised form
16 July 2019
Accepted 31 July 2019
Available online 31 July 2019

Keywords:
Graphene oxide
Amine modified graphene oxide
Buffer layer
Mesoporous perovskite solar cells

ABSTRACT

In this study, graphene oxide (GO) was synthesized via Tour method and then modified with two different amine sources that contained different branched alkyl chains. The GO and modified GOs (mGOs) with dihexylamine (DHA) and 2-ethylhexylamine (2EHA) as amine sources were used respectively as buffer layers in mixed halide mesoporous perovskite solar cells (PSCs) in order to examine whether they could improve their performance. GO and mGO samples were characterized by several techniques such as X–Ray Diffraction, X–Ray photoelectron spectroscopy (XPS), Raman analysis and thermal gravimetric analysis (TGA). The preparation of the $CH_3NH_3PbI_{3-x}Cl_x$ perovskite solution was performed using standard Schlenk techniques under argon atmosphere to attain a homogeneous coverage of the perovskite film. The solar cells with the additional layer of mGO derivatives between perovskite and hole transporting layer showed an improved overall performance compared to the reference devices which was attributed to the enhanced charge carrier transport via the mGOs. In particular, 10% increase to the overall performance of the solar cells was monitored in devices where 2-ethylhexylamine (2EHA) modified GO was used, compared to standard cell without buffer layer.

1. Introduction

In recent years, perovskite solar cells (PSCs) have attracted great attention owing to their high efficiency, low cost and easy preparation process [1,2]. Particularly, organic–inorganic hybrid perovskites follow the general formula ABX_3 (A: organic cation, *e.g.* $CH_3NH_3^+$, B: metal cation, *e.g.* Pb^{+2}, Sn^{+2}, and X: halogen anion, *e.g.* I^-, Br^-, Cl^-) and they exhibit high absorption coefficients, excellent light absorption and efficient charge injection/transport properties [3–6]. Moreover, their properties, such as the crystallinity, the bandgap and the electron–hole diffusion lengths can be tuned by utilizing appropriate A, B and X components [5,7]. By combining different halogens to synthesize mixed halide perovskites (i.e. $CH_3NH_3PbI_{3-x}Cl_x$), their stability and charge transport properties can be improved, resulting in an increase in the efficiency of PSCs [7,8]. Especially, several studies show that the use of tri-iodide ions (I_3^-) and iodine in PSCs can improve the efficiency of PSCs [9–11]. Sun et al. demonstrated that the additional I_3^- ions in organic cation solution decrease the concentration of defects in resulting perovskite films which may lead to better performing devices [10]. Apart from altering the perovskite in a PSC, changing the hole transport material (HTM) is also an alternative approach to enhance their stability [12].

Despite the major progress achieved to the overall performance of PSCs, there are still a number of issues that should be addressed for further advancing this type of solar cells before commercialization. One of them is the effect of ambient humidity during the fabrication process in general and its effect to the stability of perovskite material. Besides, the nature of electrical and electronic contact of perovskite and electrode interface is of great importance affecting the overall performance of the cell including fundamental parameters such as open circuit voltage (V_{OC}), short circuit current density (J_{SC}) and fill factor (FF) [13,14]. Free carriers are generated into perovskite after excitation, i.e. in a

* Corresponding author.
** Corresponding author.
E-mail addresses: cananvarlikli@iyte.edu.tr (C. Varlikli), estathatos@teiwest.gr (E. Stathatos).

https://doi.org/10.1016/j.renene.2019.07.162
0960-1481/

n–i–p architecture the electrons are collected by the anode and the holes are extracted from the cathode. Therefore, the electrical contact at the perovskite/electrode interface is very critical to optimize the photoconversion performance. For that reason buffer layers have been proposed as a way to improve the alignment of the electron and hole transfer materials' energy levels with that of perovskite so as to be able to tune the work function of the electrode [15–17]. Besides, buffer layers can also act as a means for enhancing the charge selectivity i.e. electron transport and hole blocking capacity while at the same time preventing the unfavorable interfacial charge recombination. Finally, buffer layers can also provide an additional advantage to stabilize the mobile ions between the perovskite grain boundaries and provide barrier protection to the halide perovskites from the ambient humidity improving the solar cell stability.

Graphene is known as a honeycomb structured material which has gained much attention in organic photonic systems (OPVs, OLEDs, OFEDs, photo–sensors) due to the extraordinary mechanical, thermal, electrochemical, magnetic and electronic properties [18–24]. Graphene derivatives, such as graphene oxide (GO) and modified graphene oxide (mGO) that are prepared via chemical synthesis method, can be dispersed in many solvents due to the presence of functional groups. Thus, it is possible to use solutions with graphene derivatives in organic photonic devices [23,24]. Recently, the graphene oxide derivatives in PSCs have been extensively studied to improve the device's efficiency and stability [25]. Functional groups on GO, rGO and mGO allow the tunning of their chemical and physical properties and can be utilized as an interlayer, dopant, HTL or buffer layer in PSCs with varying performances for the corresponding devices [26]. The use of graphene oxide as a dopant or an interlayer enhances the charge injection and charge carrier mobility which improves the PSCs' efficiency [27,28]. Mahmoudi et al. have reported that the usage of Silver-Graphene composites in perovskite active layer enhance the stability of the PSCs [29]. Moreover, the hydrophobic nature of rGO and functionalized rGOs can cause a decrement in the degradation of perovskite film through the protection of it from moisture in ambient air, while being used as a buffer layer and as a HTL on the top of the perovskite films [27,30–33]. Contrary to these beneficial effects of the graphene derivatives on PSCs, utilization of GO type as a buffer layer between perovskite and HTL was also reported to cause a decomposition in the perovskite layer under prolonged light illumination condition [25]. Consequently, the highest power conversion efficiency which has been achieved for PSCs is well over 20% by employing the rGO within MoS_2 as HTL and buffer layer [31] or by depositing rGO as a spacer layer on CuSCN based inorganic HTM layer [32].

In this study, graphene oxide (GO) was synthesized via Tour method and then modified with two different amine sources that contain different branched alkyl chains. The synthesis of $CH_3NH_3PbI_{3-x}Cl_x$ perovskite was performed using standard Schlenk techniques under argon atmosphere to obtain the better coverage of the perovskite films. The performance of PSCs based on GO and mGOs as a buffer layer between the perovskite and P3HT layers was investigated. It was found that solar cells with the additional layer of mGO derivatives present higher efficiency compared to the reference device. Improved performance of mGO derivatives can be explained by the enhanced transportation of charge carriers via the mGOs that have dot–like morphology compared to the sheet–like morphology of GO [34,35]. The utilization of mGO derivatives as buffer layer, between perovskite and HTL layer, is the state of the art and the corresponding mesoscopic PSCs have comparable PCE values with the ones reported in literature [25,27,31,36,37] for devices having similar structure as the one employed in this manuscript (Scheme 1).

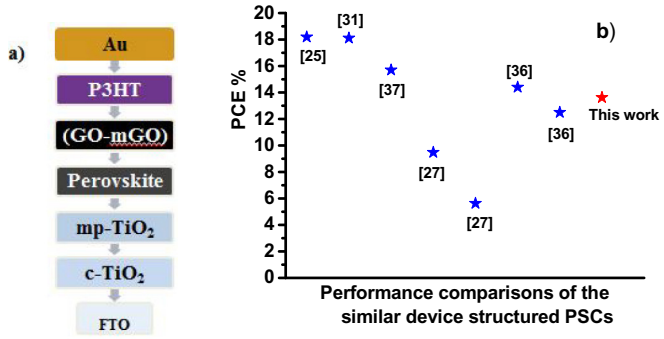

Scheme 1. a) Used device structure in this manuscript and **b)** PCE % values of PSCs reported in literature and measured in this work.

2. Experimental section and methods

2.1. Materials

Amine sources used in the synthesis of modified GOs (mGOs) [Dihexylamine (DHA) and 2-ethylhexylamine (2EHA)], ethanol, isopropyl alcohol and molecular sieve were from Sigma Aldrich. Titanium (IV) butoxide, titanium diisopropoxide bis(acetylacetonate) (75 wt% in isopropanol), 4-*tert*-butylpyridine, pluronic P123 (MW~5800 g/mol), lithium bis(trifluoromethane)sulfonimidate (Li-TFSI), chlorobenzene, dimethylformamide (DMF) were also obtained from Aldrich. Regioregular poly (3-hexylthiophene-2,5-diyl) (P3HT, 94000 g/mol) were purchased from Ossila. Lead (II) chloride was provided from Acros organics. CH_3NH_3I was prepared according to the procedure reported in literature [38]. DMF solvent was dried over molecular sieves prior to use. All other chemicals were used as received.

2.2. Measurements

Chemical structures of synthesized GO and mGO samples were characterized by the X–Ray Diffraction [XRD], Rigaku Ultima IV X–Ray Diffractometer using Cu Ka radiation, data sets were confined in the range of 3–90° (2θ), X–Ray photoelectron spectroscopy (XPS, Thermo Scientific K-Alpha Surface Analysis XPS spectrophotometer), Thermal gravimetric analysis (TGA, PerkinElmer Pyris 6 TGA) and RAMAN analysis (Horiba, XploRA) techniques. Current–voltage curves of PSCs were obtained by a Solar Simulator Solar Light (16S-300) equipped with a Xenon lamp and a Keithley 2601A sourcemeter. The morphologic structure of the $CH_3NH_3PbI_{3-x}Cl_x$ perovskite was determined by using Field Emission Scanning Electron Microscopy (FE–SEM, FEI InspectTM F50). The Electrochemical Impedance Spectroscopy (EIS) measurements were recorded using Metrohm Autolab 3. v potentiostat galvanostat (Model PGSTAT 128N). The EIS measurements were performed under dark conditions at forward bias and the frequency range which was applied was 100 kHz–0.1 Hz using a perturbation of ±10 mV. Finally, impedance data were fitted using Nova 1.10 software.

2.3. Synthesis of mGO derivatives

Graphene Oxide (GO) was synthesized according to the

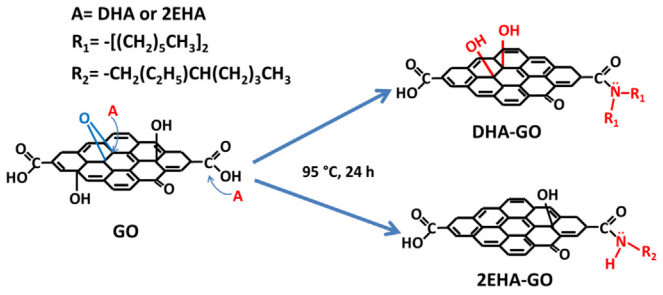

Scheme 2. Proposed binding mechanism of DHA and 2EHA on GO.

modified Hummers' method as described in our previous study [39,40]. 10 mmol of amine sources were added to 100 mL GO (2 mg/mL) aqueous dispersion and amine modification reaction was carried out at 95 °C for 24 h. The alkaline reaction solution was filtered by washing with the pure water–ethanol mixture (with 1:1 vol ratio) until the reaction medium was neutralized. This filtered solid material was dried at 70 °C for 24 h and obtained amine modified graphene oxide samples were referred as mGO. Two different amines that contain different branched alkyl chain i.e. Dihexylamine (DHA) and 2-ethylhexylamine (2EHA) were used as amine sources during the GO modification and the obtained mGO derivatives were named DHA-GO and 2EHA-GO, respectively. Then their dispersions in isopropyl alcohol (5mg/1 mL) were prepared and ultrasonicated in a water bath for 1 h before their implementation as a buffer layer between the perovskite and P3HT layers in PSCs. Proposed binding mechanism of amines on GO layer is given in Scheme 2 and further supported by the XPS, XRD and RAMAN analysis.

2.4. Preparation of $CH_3NH_3PbI_{3-x}Cl_x$ perovskite

$CH_3NH_3PbI_{3-x}Cl_x$ perovskite solution was prepared using standard Schlenk techniques under argon atmosphere. A 40 wt% mixed halide perovskite solution was prepared by mixing CH_3NH_3I and $PbCl_2$ in anhydrous DMF in a molar ratio 3:1 according to the previous reported procedure [7] except that argon atmosphere was used instead of air atmosphere during reaction.

2.5. Fabrication of the perovskite solar cells

All the processes for the device fabrication were carried out under ambient conditions of temperature and relative humidity. Glasses with a fluorine–doped tin oxide (FTO) conducting substrate (8 Ω/□, (Pilkington) were used for the fabrication of the monolithic meso–structured perovskite solar cells. The FTO glasses were patterned by chemical etching using zinc dust and HCl aqueous solution and then they were thoroughly cleaned with detergent, deionized water and acetone. A thin compact layer of TiO_2 (c–TiO_2) was deposited by spin–coating at 2000 rpm for 10 s a few drops of a solution which consisted of titanium diisopropoxide bis(acetylacetonate) diluted in isopropanol (10% v/v) followed by annealing at 500 °C for 10 min. The mesoporous TiO_2 layers (mp–TiO_2) were formed by spin–coating (1200 rpm for 20 s) a solution that was previously prepared, consisting of 0.37 mL Titanium (IV) butoxide, 0.4 mL glacial acetic acid and 0.5 g Pluronic P123 in 4 mL n–propanol, followed by sintering at 500 °C for 10 min to form porous films. These steps were repeated until the desired thickness was obtained.

For the formation of the perovskite film a small amount of the perovskite solution was spin–coated onto the photoanode films at 2000 rpm for 45 s and then the samples were placed on a hot plate at 100 °C for 30 min in order to obtain the crystalline phase of the perovskite. Subsequently the perovskite film of some of the samples was covered with a film of GO or mGO which resulted by spin–coating the corresponding solutions at 2000 rpm for 60 s and drying at 60 °C for 5 min. For the preparation of the solution for the hole transport layer (HTL), 15 mg of poly–3–hexylthiophene (P3HT) were diluted in 1 mL chlorobenzene and 7.18 mg of lithium bis(trifluoromethanesulfonyl) imide and 10.3 mg of 4–*tert*–Butylpyridine were added at the end. Prior to the deposition of the HTL the samples were left to reach room temperature. The HTL was formed by spin–coating 30 μL of the above solution at 1200 rpm for 10 s, over the perovskite films, followed by drying of the as–prepared films on a hot plate at 60 °C for 5 min. This step was repeated twice. To complete the devices' structure, gold electrode was thermally evaporated on top of the HTL. The final structure of the mesoscopic perovskite solar cells was FTO/c–TiO_2/mp–TiO_2/$CH_3NH_3PbI_{3-x}Cl_x$/(GO or mGO)/P3HT/Au (Scheme 1) and a series of three devices was fabricated for each of the different cases tested.

3. Results and discussions

3.1. Structural characterization of mGO derivatives

XPS spectra of GO, DHA-GO and 2EHA-GO are shown in Fig. 1. All of them have a broad C 1s peak that is convoluted into five characteristic sub peaks between 283 and 290 eV. Abundance of functional groups on the samples, distributions of atomic percentages of C, O and N atoms and also C:O ratio were detailed in Table 1.

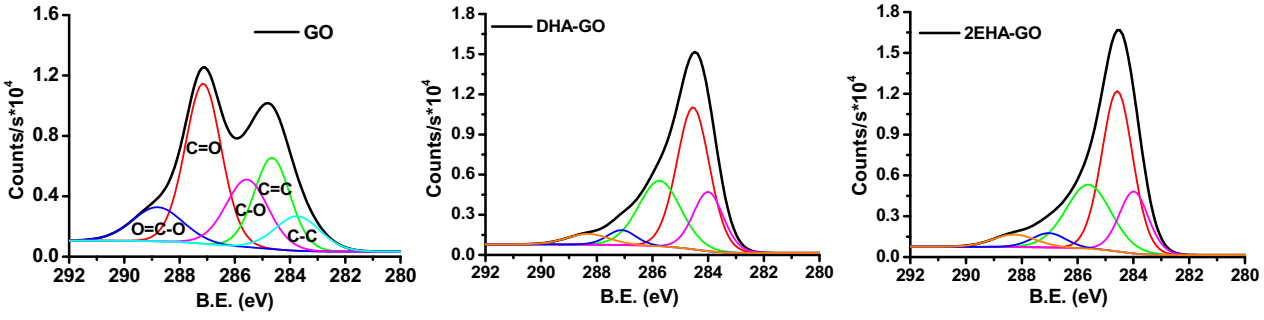

Fig. 1. C1s XPS spectra of GO, DHA-GO and 2EHA-GO samples.

Table 1
XPS and RAMAN data obtained for GO and mGO samples.

Samples		d-spacing (Å)	I_D/I_G Ratio	C1s %					At. %			C:O ratio
				sp^3 C–C	sp^2C = C	{C–OH} ∪{C–N}	{C–O–C} ∪{C=O}	O–C=O	C	O	N	
GO	8.36	0.98	10.18	21.62	18.83	38.10	11.27	68.05	31.95	–	2.13	
DHA-GO	4.39	0.94	17.68	46.15	27.44	4.22	4.50	74.56	13.43	12.01	5.55	
2EHA-GO	4.20	0.95	16.85	46.49	27.10	4.53	5.03	76.09	11.67	12.24	6.52	

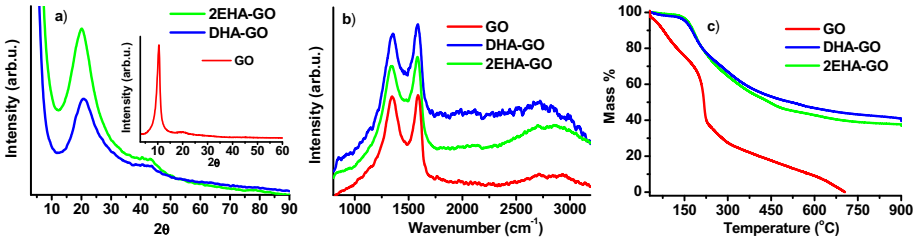

Fig. 2. Structural characterizations of GO, DHA-GO, and 2EHA-GO **a)** XRD pattern, **b)** RAMAN spectrum and **c)** TGA curves.

Compared to the GO, the existence of N atom with ~12% and, also determination of a dramatic decrement in the amounts of epoxy (C–O–C at 287.1 eV) and carboxylic acid (O=C–O; at 288.9 eV) groups on the mGO samples indicate the significant interactions between the GO and amine sources. It is thought that modification of the GO occurred through both epoxy ring opening reaction at the basal plane and amidation reaction with the carboxylic acid at the edge sides [41,42]. The XPS peaks originating from the C–N bonds are observed at around 285.5 eV and their C1s peaks overlap with the peaks of the C–OH groups in the structure [43–45]. Thus, a considerable increment in the amount of {C–OH}∪{C–N}% in mGOs demonstrates the effective amine modification on the GO layers. The C:O ratio of all of the synthesized mGO derivatives are higher than that of the GO, which points out that the used amines not only modified the surface but also caused partial reduction of GO [46]. This situation is supported with the sp^2 C=C%s of around 46%. Significant increase in the abundance of sp^3 C–C%s for the mGO samples compared to the GO is attributed to the contribution of alkyl chains in the amine groups.

Characteristic XRD peak (2θ) at around 10° of GO completely shifted to ~ 20° (2θ) after amine modification (Fig. 2a). Negligible peak at 43°(2θ) belongs to (100) crystal orientation of graphite and addresses the non–uniform crystal structure obtained by the modification of GO surface with amine groups [46]. While the $-NH_2$ groups of the amine sources in the alcaline character directly attack the epoxy carbon in the basal plane of the GO to perform the ring opening reaction, the conjugated acids formed in the medium provide the acidic environment required for elimination, and thus reduce the GO to large extent. Shorter interlayer distances (d-spacing) of 2EHA-GO and DHA-GO compared to the GO may be attributed to this situation (Table 1). Additionally, this lower d-spacing values, which are determined contrary to expectations for mGOs, may explaine that high density hydrocarbons chains being selectively parallel positioned at the edge side of GO plane due to the steric hindrances [42].

RAMAN spectroscopy is an important analysing technique for the graphite like materials. Specific D bands at around 1350 cm^{-1} and D bands at around 1585 cm^{-1} are clearly observed for all samples (Fig. 2b). The G band peaks of the 2EHA-GO (1582.7 cm^{-1}) and DHA-GO (1585.7 cm^{-1}) are detected to shift through to the lower frequency (red shift) compared to the GO (1588.0 cm^{-1}). This situation can be attributed to the fact that amine sources with long alkyl chains behave as electron donor due to the formation of positive inductive effects on the amine group attached to the GO surface. It is known that electron donor or acceptor properties of the nitrogen–containing dopants vary depending on their bonding conformation to the GO surface [47]. Additionally, the quality of the graphene derivatives can be determined according to the Raman I_D/I_G ratio. Given the fact that the I_D/I_G ratio was approximately the same for the GO and mGOs it denotes that the modification reactions of GO occur on the sp^3 C–C sides predominantly, and the graphitic carbons (sp^2 C=C regions) are to a large extent preserved (Table 1).

Fig. 2c illustrates the TGA curves of the GO and mGO samples. Contrary to the GO (15.24%), the negligible mass losses for the mGO derivatives below 100 °C (~1–2%) clearly indicate the hydrophobic characters of those derivatives [42]. Unlike the GO, no sharp mass losses were detected for the mGOs between 100°C and 300 °C. This can be explained by the removal of the oxygenated functional groups from their structure after the modification reactions. Furthermore, the slight mass losses which were observed for the mGO derivatives at the same temperature range demonstrate the self decomposition of the amine groups which interact with the GO physically [42,48,49]. Notable increment in the thermal stability was observed for both 2EHA-GO and DHA-GO samples as compared with the GO.

4. Surface morphology characterization of the GO and mGO buffer layers

Top view SEM images (Fig. 3a–c) were obtained in order to evaluate the quality of the formed GO or mGO buffer layers over the perovskite films. The GO solution formed a dense film without however covering the underlying perovskite film homogeneously, while both the mGO solutions formed porous films with full coverage. The formation of a porous buffer layer could be proven to be an advantage for the deposition of the hole transport material, facilitating the hole transport and confining the charge recombination improving at the same time the overall performance of the final perovskite devices. Cross section image of standard

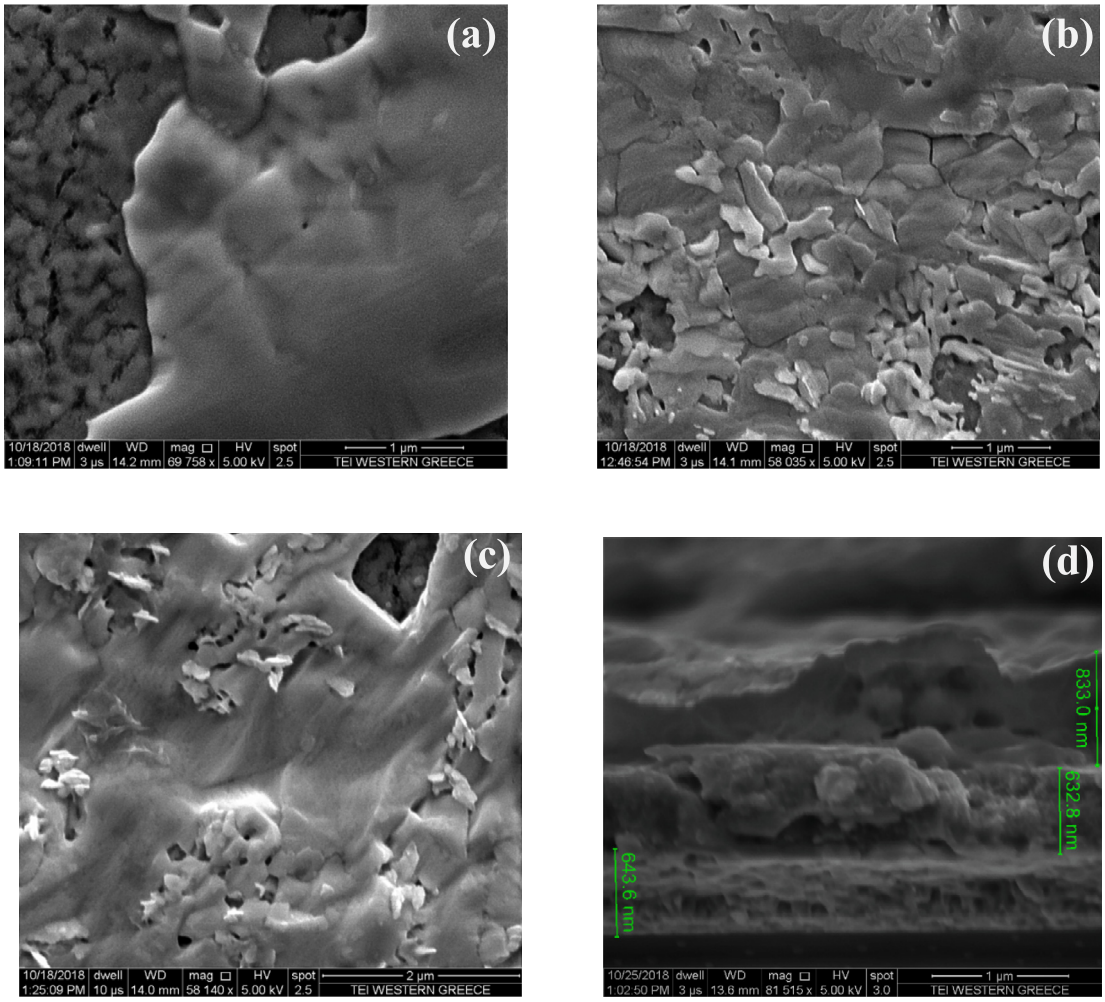

Fig. 3. SEM images (top view) of the surface morphology of the perovskite film having a buffer layer of **a)** GO **b)** DHA-GO or **c)** 2EHA-GO. **d)** Cross section image of standard configuration of PSC with mesoporous titania film (632 nm) and perovskite layer on the top (833 nm).

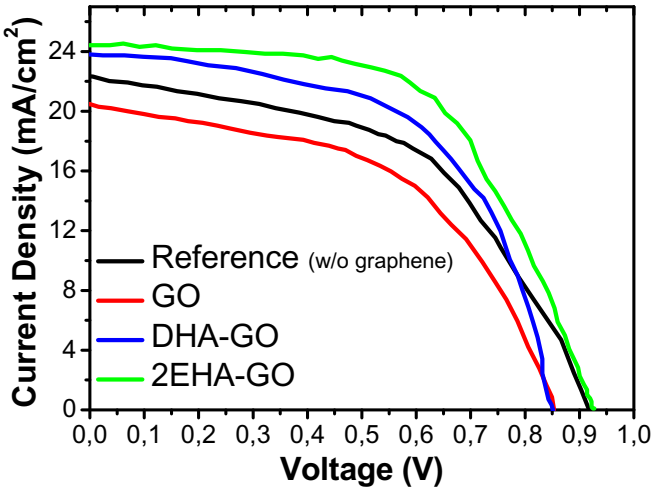

Fig. 4. The J–V characteristic curve for the perovskite solar cells measured with forward scan (from short circuit to open circuit) with delay = 40 ms.

configuration of PSC showed an average thickness for mesoporous TiO_2 film around 632 nm and for perovskite layer on the top about 833 nm.

Table 2
Solar cell parameters for the PSCs with and without the presence of GO or mGO buffer layer.

Samples	J_{SC} (mA/cm^2)	V_{OC} (V)	n (%)	FF
Reference	22.34	0.92	10.56	0.51
GO	20.49	0.85	8.96	0.51
DHA-GO	23.84	0.85	11.55	0.57
2EHA-GO	24.43	0.93	13.25	0.58

4.1. Characterization of perovskite solar cells

The perovskite solar cells with and without the GO or mGOs buffer layer were electrically characterized and the current density–photovoltage (J–V) characteristic curves are presented in Fig. 4 while the obtained electrical parameters are summarized in Table 2. In general the addition of the mGO buffer layers, namely DHA-GO and 2EHA-GO improved the short–circuit current density (J_{SC}), the fill factor (FF) and the overall power conversion efficiency of the PSCs, whereas the GO buffer layer reduced all the electrical parameters of the final devices compared with the ones used as a reference without any buffer layer. The increase of the J_{SC} for the samples employing DHA-GO and 2EHA-GO buffer layers was attributed to the uniformity of the layer over the perovskite film which we assumed that obstructed the formation of shunt paths

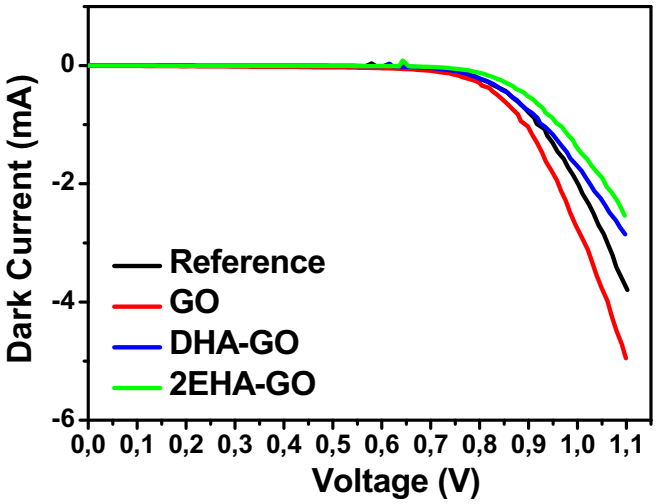

Fig. 5. Dark current–voltage characteristic curves for the perovskite solar cells with and without the presence of GO or mGO buffer layer.

which could enhance the charge recombination and also have a negative effect on the FF. On the other hand, hydrophilic nature of the GO due to the oxygenated functional groups on its structure stimulates interactions between perovskite layer and air moisture. These interactions lead to perovskite decomposition and therefore to decrement in performances of PSCs [25].

The reduction of the charge recombination by utilizing the mGO buffer layer can also be reflected as a confinement of the dark current (Fig. 5). Since the open circuit voltage of the PSCs was more or less the same with small discrepancies no major differences are expected to the dark current. In fact the curves for all the fabricated devices didn't display substantial differences with the curve corresponding to the sample with the 2EHA-GO buffer layer just exhibiting a slightly smaller decreasing rate for the voltage.

Electrochemical impedance spectroscopy measurements were performed for the fabricated devices with and without the presence of the GO or mGOs buffer layer. Fig. 6 (a) presents the obtained EIS plots (Nyquist plots) of the PSCs where the experimental data are represented by symbols, while each fitted plot is represented by a line and Fig. 6 (b) depicts the simplified equivalent circuit used in order to fit the obtained experimental data. The element in Fig. 6 (b)

Table 3
Electrochemical impedance spectroscopy fitted parameters.

Samples	R_S (Ω)	R_{REC} (Ω)	$C_1{*}10^{-6}$ (F)	R_{HTM} (Ω)	$C_2{*}10^{-6}$ (F)
Reference	39.60	492	2.68	2530	3.26
GO	55.3	831	1.93	878	0.19
DHA-GO	61	3210	3.87	853	1.14
2EHA-GO	51.4	1090	3.86	2970	7.51

depending on the parameters Y_o and N which is in parallel with a resistance is called a constant phase element (CPE) and can be converted to a capacitance element. In the Nyquist plots, instead of getting two distinct semicircles, each one assigned to the parallel combination of the resistance with the CPE element, only one merged semi–arc can be observed representing both parallel branches. One of the parallel branches and the corresponding electrochemical parameters are related to the HTM/gold interface and its charge transfer properties, while the other one is related to the recombination processes which take place at the ETL/perovskite interface. Moreover, the resistance in high frequencies (R_S) is related to the series resistance of the solar cell. All the fitted parameters are summarized in Table 3. The larger values of the R_{REC} obtained for the solar cells employing the mGO buffer layer indicate suppressed recombination processes, namely charges are harder to transfer from the ETL/perovskite interface which corroborate our initial assumption that the addition of the buffer layer can help in the reduction of the charge recombination.

5. Conclusions

In summary, graphene oxide (GO) was synthesized and subsequently modified using two different amine sources having different branched alkyl chains. The GO and modified GOs (mGOs) were applied as buffer layers in mixed halide $CH_3NH_3PbI_{3-x}Cl_x$ mesoporous perovskite solar cells. The solar cells having the additional mGO buffer layer displayed improved performance compared with the reference devices and the ones employing the GO buffer layer, which was ascribed to the formation of a uniform porous mGO film which probably facilitated the deposition of the hole transport material and assisted in the reduction of the charge recombination. In addition, the hydrophobic character that the mGO derivatives demonstrated could provide an extra shield of the perovskite film from the humidity and air elongating the stability of the fabricated PSCs.

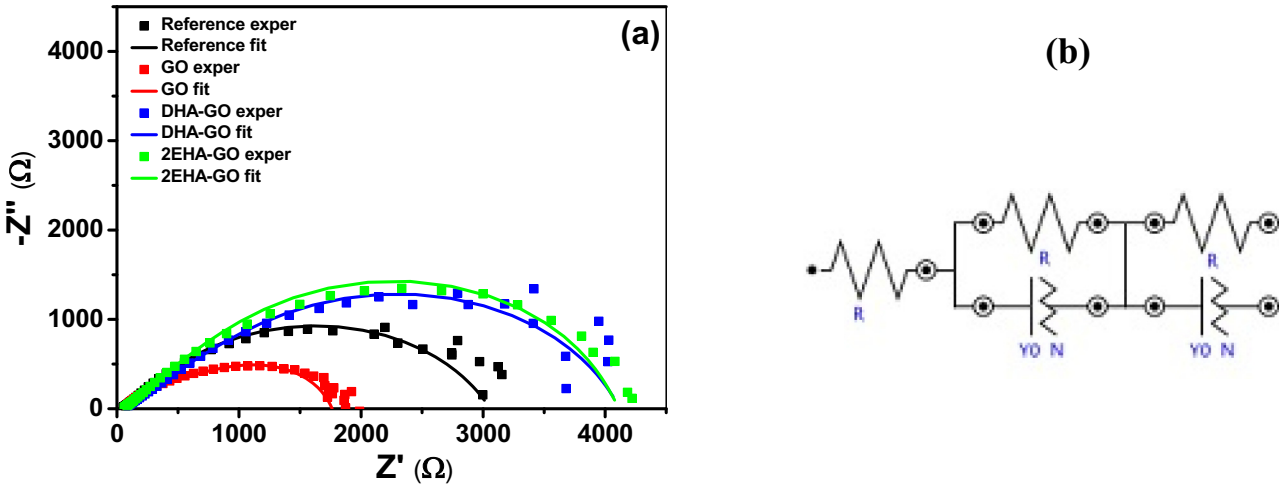

Fig. 6. (a) Electrochemical impedance spectroscopy plots of the PSCs measured under dark conditions and (b) equivalent circuit used to fit the experimental data.

Acknowledgments

The authors would like to greatly acknowledge the contribution of Dr. Alexandros Kalarakis in the collection of the FE-SEM images. Dimitra Sygkridou and Elias Stathatos would like acknowledge that this work was co-funded by the European Union and the General Secretariat of Research and Technology, Ministry Of Education, Research Religious Affairs under the project "PrintPero" of the Bilateral R&T Cooperation Program Greece-Germany 2018–2021 (project code: Τ2ΔΓΕ-0560, MIS: 5030132). This support is gratefully acknowledged.

H. Diker and C. Varlikli acknowledge the research project funds of Scientific and Technological Research Council of Turkey (TUBITAK) (Project #: 114M508).

References

[1] J. Chang, Z. Lin, H. Zhu, F.H. Isikgor, Q.-H. Xu, C. Zhang, Y. Hao, J. Ouyang, Enhancing the photovoltaic performance of planar heterojunction perovskite solar cells by doping the perovskite layer with alkali metal ions, J. Mater. Chem. A. 4 (2016) 16546–16552, https://doi.org/10.1039/C6TA06851K.

[2] H. Kim, J.S. Han, J. Choi, S.Y. Kim, H.W. Jang, Halide perovskites for applications beyond photovoltaics, Small Methods 2 (2018) 1700310, https://doi.org/10.1002/smtd.201700310.

[3] S.-H. Kim, A. Kirakosyan, J. Choi, J.H. Kim, Spectroscopic study on the interaction of organic-inorganic hybrid perovskite nanoparticles with linear aliphatic alcohols, Dyes Pigments 143 (2017) 71–75, https://doi.org/10.1016/J.DYEPIG.2017.04.033.

[4] Y. Wang, T. Zhang, G. Li, F. Xu, T. Wang, Y. Li, Y. Yang, Y. Zhao, A mixed-cation lead iodide $MA_{1-x}EA_xPbI_3$ absorber for perovskite solar cells, J. Energy Chem. 27 (2018) 215–218, https://doi.org/10.1016/J.JECHEM.2017.09.027.

[5] M. Su, D. Wu, B. Fan, F. Wang, K. Wang, Z. Luo, Synthesis of highly efficient and stable $CH_3NH_3PbBr_3$ perovskite nanocrystals within mesoporous silica through excess CH_3NH_3Br method, Dyes Pigments 155 (2018) 23–29, https://doi.org/10.1016/J.DYEPIG.2018.02.010.

[6] D.Y. Wan, Y.L. Zhao, Y. Cai, T.C. Asmara, Z. Huang, J.Q. Chen, J. Hong, S.M. Yin, C.T. Nelson, M.R. Motapothula, B.X. Yan, D. Xiang, X. Chi, H. Zheng, W. Chen, R. Xu, Ariando, A. Rusydi, A.M. Minor, M.B.H. Breese, M. Sherburne, M. Asta, Q.-H. Xu, T. Venkatesan, Electron transport and visible light absorption in a plasmonic photocatalyst based on strontium niobate, Nat. Commun. 8 (2017) 15070, https://doi.org/10.1038/ncomms15070.

[7] A. Apostolopoulou, D. Sygkridou, A. Rapsomanikis, A.N. Kalarakis, E. Stathatos, Enhanced performance of mesostructured perovskite solar cells in ambient conditions with a composite TiO_2–In_2O_3 electron transport layer, Sol. Energy Mater. Sol. Cells 166 (2017), https://doi.org/10.1016/j.solmat.2017.03.024.

[8] Y. Pei, X. Zou, Y. Guan, G. Teng, Effect of codoping Cl anion and 5-AVA cation on performance of large-area perovskite solar cells with double-mesoporous layers, Int. J. Photoenergy (2016) 1–11, https://doi.org/10.1155/2016/2953592, 2016.

[9] W.S. Yang, B.-W. Park, E.H. Jung, N.J. Jeon, Y.C. Kim, D.U. Lee, S.S. Shin, J. Seo, E.K. Kim, J.H. Noh, S. Il Seok, Iodide management in formamidinium-lead-halide-based perovskite layers for efficient solar cells, Science 356 (2017) 1376–1379, https://doi.org/10.1126/science.aan2301.

[10] Q. Sun, X. Gong, H. Li, S. Liu, X. Zhao, Y. Shen, M. Wang, Direct formation of I_3^- ions in organic cation solution for efficient perovskite solar cells, Sol. Energy Mater. Sol. Cells 185 (2018) 111–116, https://doi.org/10.1016/J.SOLMAT.2018.05.017.

[11] M. Wang, Z. Zang, B. Yang, X. Hu, K. Sun, L. Sun, Performance improvement of perovskite solar cells through enhanced hole extraction: the role of iodide concentration gradient, Sol. Energy Mater. Sol. Cells 185 (2018) 117–123, https://doi.org/10.1016/J.SOLMAT.2018.05.025.

[12] Y. Di, Q. Zeng, C. Huang, D. Tang, K. Sun, C. Yan, Y. Wang, S. Ke, L. Jiang, X. Hao, Y. Lai, F. Liu, Thermal-evaporated selenium as a hole-transporting material for planar perovskite solar cells, Sol. Energy Mater. Sol. Cells 185 (2018) 130–135, https://doi.org/10.1016/J.SOLMAT.2018.05.022.

[13] J. Xiong, B. Yang, C. Cao, R. Wu, Y. Huang, J. Sun, J. Zhang, C. Liu, S. Tao, Y. Gao, J. Yang, Interface degradation of perovskite solar cells and its modification using an annealing-free TiO_2 NPs layer, Org. Electron. 30 (2016) 30–35, https://doi.org/10.1016/J.ORGEL.2015.12.010.

[14] Z. Zhou, S. Pang, Z. Liu, H. Xu, G. Cui, Interface engineering for high-performance perovskite hybrid solar cells, J. Mater. Chem. A. 3 (2015) 19205–19217, https://doi.org/10.1039/C5TA04340A.

[15] Q. Sun, S. Zhou, X. Shi, X. Wang, L. Gao, Z. Li, Y. Hao, Efficiency enhancement of perovskite solar cells via electrospun CuO nanowires as buffer layers, ACS Appl. Mater. Interfaces 10 (2018) 11289–11296, https://doi.org/10.1021/acsami.7b19335.

[16] W.K. Lin, S.H. Su, M.C. Yeh, C.Y. Chen, M. Yokoyama, Enhancing efficiency of perovskite solar cells using a thin buffer layer, Vacuum 140 (2017) 82–88, https://doi.org/10.1016/J.VACUUM.2016.12.037.

[17] E. Stratakis, M.M. Stylianakis, E. Koudoumas, E. Kymakis, Plasmonic organic photovoltaic devices with graphene based buffer layers for stability and efficiency enhancement, Nanoscale 5 (2013) 4144, https://doi.org/10.1039/c3nr00656e.

[18] T.D. Dao, H.M. Jeong, Graphene prepared by thermal reduction–exfoliation of graphite oxide: effect of raw graphite particle size on the properties of graphite oxide and graphene, Mater. Res. Bull. 70 (2015) 651–657, https://doi.org/10.1016/J.MATERRESBULL.2015.05.038.

[19] C. Botas, P. Álvarez, C. Blanco, R. Santamaría, M. Granda, P. Ares, F. Rodríguez-Reinoso, R. Menéndez, The effect of the parent graphite on the structure of graphene oxide, Carbon N. Y. 50 (2012) 275–282, https://doi.org/10.1016/J.CARBON.2011.08.045.

[20] S. Bak, D. Kim, H. Lee, Graphene quantum dots and their possible energy applications: a review, Curr. Appl. Phys. 16 (2016) 1192–1201, https://doi.org/10.1016/J.CAP.2016.03.026.

[21] P.J. Jesuraj, R. Parameshwari, K. Kanthasamy, J. Koch, H. Pfnür, K. Jeganathan, Hole injection enhancement in organic light emitting devices using plasma treated graphene oxide, Appl. Surf. Sci. 397 (2017) 144–151, https://doi.org/10.1016/J.APSUSC.2016.11.110.

[22] F. Bonaccorso, Z. Sun, T. Hasan, A.C. Ferrari, Graphene photonics and optoelectronics, Nat. Photonics 4 (2010) 611–622, https://doi.org/10.1038/nphoton.2010.186.

[23] Q. Liu, Z. Liu, X. Zhang, N. Zhang, L. Yang, S. Yin, Y. Chen, Organic photovoltaic cells based on an acceptor of soluble graphene, Appl. Phys. Lett. 92 (2008) 223303, https://doi.org/10.1063/1.2938865.

[24] Y. Gao, H.-L. Yip, K.-S. Chen, K.M. O'Malley, O. Acton, Y. Sun, G. Ting, H. Chen, A.K.-Y. Jen, Surface doping of conjugated polymers by graphene oxide and its application for organic electronic devices, Adv. Mater. 23 (2011) 1903–1908, https://doi.org/10.1002/adma.201100065.

[25] A. Agresti, S. Pescetelli, B. Taheri, A.E. Del Rio Castillo, L. Cinà, F. Bonaccorso, A. Di Carlo, Graphene-perovskite solar cells exceed 18% efficiency: a stability study, ChemSusChem 9 (2016) 2609–2619, https://doi.org/10.1002/cssc.201600942.

[26] C. Ciceroni, A. Agresti, A. Di Carlo, F. Brunetti, Graphene oxide for DSSC, OPV and perovskite stability, Futur. Semicond. Oxides Next-Gen. Sol. Cells (2018) 503–531, https://doi.org/10.1016/B978-0-12-811165-9.00013-2.

[27] Q. Luo, Y. Zhang, C. Liu, J. Li, N. Wang, H. Lin, Iodide-reduced graphene oxide with dopant-free spiro-OMeTAD for ambient stable and high-efficiency perovskite solar cells, J. Mater. Chem. A. 3 (2015) 15996–16004, https://doi.org/10.1039/C5TA02710A.

[28] G.S. Han, Y.H. Song, Y.U. Jin, J.-W. Lee, N.-G. Park, B.K. Kang, J.-K. Lee, I.S. Cho, D.H. Yoon, H.S. Jung, Reduced graphene oxide/mesoporous TiO_2 nanocomposite based perovskite solar cells, ACS Appl. Mater. Interfaces 7 (2015) 23521–23526, https://doi.org/10.1021/acsami.5b06171.

[29] T. Mahmoudi, Y. Wang, Y.-B. Hahn, Stability enhancement in perovskite solar cells with perovskite/silver–graphene composites in the active layer, ACS Energy Lett. 4 (2019) 235–241, https://doi.org/10.1021/acsenergylett.8b02201.

[30] A.L. Palma, L. Cinà, S. Pescetelli, A. Agresti, M. Raggio, R. Paolesse, F. Bonaccorso, A. Di Carlo, Reduced graphene oxide as efficient and stable hole transporting material in mesoscopic perovskite solar cells, Nano Energy 22 (2016) 349–360, https://doi.org/10.1016/J.NANOEN.2016.02.027.

[31] L. Najafi, B. Taheri, B. Martín-García, S. Bellani, D. Di Girolamo, A. Agresti, R. Oropesa-Nuñez, S. Pescetelli, L. Vesce, E. Calabrò, M. Prato, A.E. Del Rio Castillo, A. Di Carlo, F. Bonaccorso, MoS_2 quantum dot/graphene hybrids for advanced interface engineering of a $CH_3NH_3PbI_3$ perovskite solar cell with an efficiency of over 20%, ACS Nano 12 (2018) 10736–10754, https://doi.org/10.1021/acsnano.8b05514.

[32] N. Arora, M.I. Dar, A. Hinderhofer, N. Pellet, F. Schreiber, S.M. Zakeeruddin, M. Grätzel, Perovskite solar cells with CuSCN hole extraction layers yield stabilized efficiencies greater than 20, Science 358 (2017) 768–771, https://doi.org/10.1126/science.aam5655.

[33] E.L. Lim, C.C. Yap, M.H.H. Jumali, M.A.M. Teridi, C.H. Teh, A mini review: can graphene Be a novel material for perovskite solar cell applications? Nano-Micro Lett. 10 (2018) 27, https://doi.org/10.1007/s40820-017-0182-0.

[34] J. Kyu Kim, S. Bae, Y. Yi, M. Jin Park, S. Jin Kim, N. Myoung, C.-L. Lee, B. Hee Hong, J. Hyeok Park, Origin of white electroluminescence in graphene quantum dots embedded host/guest polymer light emitting diodes, Sci. Rep. 5 (2015) 11032, https://doi.org/10.1038/srep11032.

[35] W. Kwon, Y.-H. Kim, C.-L. Lee, M. Lee, H.C. Choi, T.-W. Lee, S.-W. Rhee, Electroluminescence from graphene quantum dots prepared by amidative cutting of tattered graphite, Nano Lett. 14 (2014) 1306–1311, https://doi.org/10.1021/nl404281h.

[36] E. Nouri, Y.-L. Wang, Q. Chen, J.-J. Xu, G. Paterakis, V. Dracopoulos, Z.-X. Xu, D. Tasis, M.R. Mohammadi, P. Lianos, Introduction of graphene oxide as buffer layer in perovskite solar cells and the promotion of soluble n-Butyl-substituted copper phthalocyanine as efficient hole transporting material, Electrochim. Acta 233 (2017) 36–43, https://doi.org/10.1016/J.ELECTACTA.2017.03.027.

[37] X. Hu, H. Jiang, J. Li, J. Ma, D. Yang, Z. Liu, F. Gao, S. (Frank) Liu, Air and thermally stable perovskite solar cells with CVD-graphene as the blocking layer, Nanoscale 9 (2017) 8274–8280, https://doi.org/10.1039/C7NR01186E.

[38] M.M. Lee, J. Teuscher, T. Miyasaka, T.N. Murakami, H.J. Snaith, Efficient hybrid solar cells based on meso-superstructured organometal halide perovskites, Science 338 (2012) 643–647, https://doi.org/10.1126/science.1228604 (80-.).

[39] W.S. Hummers, R.E. Offeman, Preparation of graphitic oxide, J. Am. Chem. Soc.

80 (1958) 1339, https://doi.org/10.1021/ja01539a017.
[40] H. Diker, G.B. Durmaz, H. Bozkurt, F. Yeşil, C. Varlikli, Controlling the distribution of oxygen functionalities on GO and utilization of PEDOT:PSS-GO composite as hole injection layer of a solution processed blue OLED, Curr. Appl. Phys. 17 (2017), https://doi.org/10.1016/j.cap.2017.02.002.
[41] W. Li, X.Z. Tang, H.B. Zhang, Z. Jiang, Z.Z. Yu, X.S. Du, Y.W. Mai, Simultaneous surface functionalization and reduction of graphene oxide with octadecylamine for electrically conductive polystyrene composites, Carbon N. Y. 49 (2011) 4724–4730, https://doi.org/10.1016/j.carbon.2011.06.077.
[42] A.M. Shanmugharaj, J.H. Yoon, W.J. Yang, S.H. Ryu, Synthesis, characterization, and surface wettability properties of amine functionalized graphene oxide films with varying amine chain lengths, J. Colloid Interface Sci. 401 (2013) 148–154, https://doi.org/10.1016/j.jcis.2013.02.054.
[43] C. Botas, P. Álvarez, C. Blanco, M.D. Gutiérrez, P. Ares, R. Zamani, J. Arbiol, J.R. Morante, R. Menéndez, Tailored graphene materials by chemical reduction of graphene oxides of different atomic structure, RSC Adv. 2 (2012) 9643–9650, https://doi.org/10.1039/c2ra21447d.
[44] S. Stankovich, D.A. Dikin, R.D. Piner, K.A. Kohlhaas, A. Kleinhammes, Y. Jia, Y. Wu, S.T. Nguyen, R.S. Ruoff, Synthesis of graphene-based nanosheets via chemical reduction of exfoliated graphite oxide, Carbon N. Y. 45 (2007) 1558–1565, https://doi.org/10.1016/j.carbon.2007.02.034.
[45] J. Wang, T. Zhou, H. Deng, F. Chen, K. Wang, Q. Zhang, Q. Fu, An environmentally friendly and fast approach to prepare reduced graphite oxide with water and organic solvents solubility, Colloids Surfaces B Biointerfaces 101 (2013) 171–176, https://doi.org/10.1016/j.colsurfb.2012.06.008.
[46] H. Pan, X. Wang, Y. Zhang, L. Yu, Z. Zhang, Graphene oxides reduced and modified by hydramines - potentials as electrode materials of supercapacitors and reinforcing agents of waterborne polyurethane, Mater. Res. Bull. 59 (2014) 117–124, https://doi.org/10.1016/j.materresbull.2014.07.010.
[47] S.H. Ryu, A.M. Shanmugharaj, Influence of long-chain alkylamine-modified graphene oxide on the crystallization, mechanical and electrical properties of isotactic polypropylene nanocomposites, Chem. Eng. J. 244 (2014) 552–560, https://doi.org/10.1016/j.cej.2014.01.101.
[48] O.C. Compton, D.A. Dikin, K.W. Putz, L.C. Brinson, S.T. Nguyen, Electrically conductive “alkylated” graphene paper via chemical reduction of amine-functionalized graphene oxide paper, Adv. Mater. 22 (2010) 892–896, https://doi.org/10.1002/adma.200902069.
[49] F. Liu, L. Wu, Y. Song, W. Xia, K. Guo, Effect of molecular chain length on the properties of amine-functionalized graphene oxide nanosheets/epoxy resins nanocomposites, RSC Adv. 5 (2015) 45987–45995, https://doi.org/10.1039/C5RA02013A.